Int. J. Heat Mass Transfer. Vol. 23, pp. 1493–1503
© Pergamon Press Ltd. 1980. Printed in Great Britain

0017–9310/80/1101–1493 $02.00/0

HEAT TRANSFER AT THE SOLID–LIQUID INTERFACE DURING MELTING FROM A HORIZONTAL CYLINDER

A. G. BATHELT* and R. VISKANTA

Heat Transfer Laboratory, School of Mechanical Engineering,
Purdue University, West Lafayette, IN 47907, U.S.A.

(*Received* 25 *January* 1980 *and in revised form* 21 *March* 1980)

Abstract – Heat transfer during melting from a horizontal cylindrical heat source with a uniform surface heat flux (heated electrically) and a uniform surface temperature (heated by circulating a fluid through a multipass heat exchanger) embedded in *n*-paraffins (*n*-heptadecane and *n*-octadecane) have been studied experimentally. The instantaneous shape of the melt volume was recorded photographically and local heat transfer coefficients at the solid–liquid interface, determined from these data, are presented. For quasi-steady melting, the local and average heat transfer results are correlated in dimensionless form. Using the correlation thus determined, the solid–liquid interface position was calculated and found to be in good agreement with experimental data.

NOMENCLATURE

c, specific heat;
D_0, diameter of the cylinder;
Fo, Fourier number, $\alpha_l t/R_0^2$;
Fo_0, Fourier number, $\alpha_l t_0/R_0^2$;
Gr, Grashof number, $g\beta(T_w - T_f)R_c^3/\nu_l^2$;
g, gravitational constant;
h, local heat transfer coefficient based on cylinder surface minus fusion temperature difference;
Δh_f, latent heat of fusion;
k, thermal conductivity;
L, length of the cylinder;
Nu, Nusselt number, hD_0/k_l;
Nu_{R_c}, Nusselt number, hR_c/k_l;
Pr, Prandtl number, ν_l/α_l;
q_w, heat flux at the cylinder surface;
r, radial distance;
r_0, radial distance, defined by equation (7);
r_m, mean radius of solid–liquid interface position, $(1/2\pi)\int_0^{2\pi} r\,d\theta$;
R, radius of the cylinder;
R_c, characteristic radius for correlating heat transfer data, defined by equation (5);
Ra, Rayleigh number, $GrPr$;
S, subcooling parameter, $c_s(T_f - T_i)/\Delta h_f$;
Ste_T, Stefan number for constant cylinder surface temperature, $c_l(T_w - T_f)/\Delta h_f$;
Ste_I, Stefan number at the solid–liquid interface, $c_l(T_w - T_f)/\Delta h_f$;
Ste_H, Stefan number for constant cylinder surface heat flux, $c_l q_w R_0/k\Delta h_f$;
t, time;
t_0, time at which natural convection begins to develop;
T, temperature.

Greek symbols

α_l, thermal diffusivity, $k_l/\rho_l c_l$;
β, thermal expansion coefficient;
θ, angle, see Fig. 6;
ρ, mass density;
τ_0, dimensionless time, $Ste_I Fo_0$;
τ_I, dimensionless time, $Ste_I Fo$;
τ_H, dimensionless time, $Ste_H Fo$;
ν, kinematic viscosity.

Subscripts

f, fusion (melting);
i, initial;
l, liquid;
s, solid;
w, wall.

Superscripts

*, normalized with respect to the cylinder radius;
–, circumferentially averaged heat transfer coefficient.

INTRODUCTION

RECENT experimental studies have conclusively established that only during the early stages of melting from horizontal [1–6] and vertical [7, 8] heat sources is heat transfer in the liquid by conduction. With continued melting and increase in size of the melt volume, natural convection flow develops in the liquid and at later times heat transfer by convection predominates over conduction. Both instantaneous local and circumferentially averaged heat transfer coefficients at the heat

*Present address: Dornier-System GmbH, 7990 Friedrichshafen, West Germany.

source surface during melting from single [1–3] and multiple [5, 6] horizontal cylinders embedded in a phase change material have been measured and reported. Heat transfer at the solid–liquid interface during melting has received little attention [8–10]. Instantaneous local heat transfer coefficients during melting of *n*-octadecane from a vertical wall have been determined [8], and heat flux at the solid–liquid interface in naphthalene, as a function of time and angular position, was recently reported [9]. This latter study used experimental techniques nearly identical to those of the earlier works and was brought to the authors' attention by one of the referees. However, no heat transfer coefficient data or correlations are included in the paper. The work reported here complements and extends the published results.

The purpose of this paper is to report on an experimental study to determine heat transfer at the solid–liquid interface during melting. The work was motivated by the need for basic information required to predict the position of the phase-change boundary in designing latent heat-of-fusion thermal energy storage (TES) systems. The concept has the primary advantage of performing the storage function at nearly constant temperature and a large specific storage capacity [11]. Good understanding of heat transfer processes involved is essential for predicting the system performance with accuracy under realistic demand conditions of charging and discharging and thus avoiding costly system overdesign. Commercial acceptance and economics of solar energy, conservation, "waste" heat utilization and other alternate energy technologies are tied to the design and development of efficient and cost effective TES systems.

Heat transfer at the solid–liquid interface during melting from a horizontal cylindrical heat source embedded in a phase change material is studied because a class of storage units given serious consideration is a standard shell and tube heat exchanger with the PCM on the shell side. Experiments during melting from a heat source with a uniform surface heat flux and uniform temperature boundary conditions have been performed. The solid–liquid interface position has been recorded photographically and from these data local heat transfer coefficients have been determined at the interface for paraffins (*n*-heptadecane, $C_{17}H_{36}$, $T_f = 22.2°C$ and *n*-octadecane, $C_{18}H_{38}$, $T_f = 28.2°C$) as phase change materials.

EXPERIMENTS

Test apparatus

Two similar rectangular test cells, in which melting occurred essentially in two directions, were designed and built. The test cell described here was used for the constant heat input experiments, and had inside dimensions of $16.2 \times 13.2 \times 4.0$ cm, while the larger second test cell ($35.5 \times 25.5 \times 7.5$ cm) was employed for the constant surface temperature experiments.

The U-shaped aluminum frame, 4.0 cm thick, consisting of two vertical and one horizontal parts, was attached to a rectangular base plate which could be adjusted in the vertical direction at its four corners for precise leveling. The front and back sides of the cell were made of 0.6 cm thick plate glass, to allow for visualization, photographing and optical observation of the phenomena taking place during phase transformation. A cut-away top view of the test cell is shown in Fig. 1. Except for the size, number and location of thermocouples, the two cells were identical. Detailed description of the test apparatus is available elsewhere [10].

The sealing was accomplished by placing a thin rubber gasket between the glass plate and the main frame. To attain uniform pressure along the two vertical and the lower horizontal edges of the glass plate, a collar was machined in the aluminum frame on each side to accommodate an aluminum stress-relief strip which was pressed against the edges of the glass plate by a number of screws along the U-shape.

To reduce natural convection from the test cell a second glass plate was installed parallel to the first one. The air gap (1 cm) between the two vertical glass plates was so selected as to minimize heat transfer between the test cell and the ambient environment. The top of the test cell was closed with a Plexiglass cover. A frosted glass screen was hinged to this cover which could be turned by 180° and placed parallel to the window facing the camera when the solid–liquid interface was photographed.

A 1.9 cm O.D. brass tube with a snugly fitted electrical cartride heater (0.64 cm O.D.) served as a constant heat input source. The cylinder was installed horizontally in the test cell with its axis perpendicular to the glass walls of the test cell. Small diameter holes, 0.1 I.D. were drilled axially at $\theta = 0°$, 90°, 180° and 270°, and radially at $1/4\,L$, $1/2\,L$ and $3/4\,L$ in the brass tube wall to accommodate the Chromel–Constantan (Type E) thermocouple wires. After the thermocouple junctions were brought to the surface and soldered, the cylinder surface was polished. A rectangular groove machined radially at one end of the brass tube

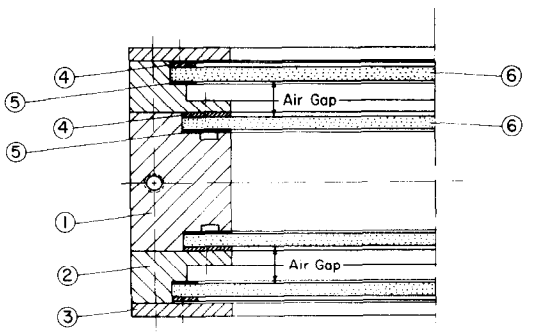

FIG. 1. Cut-away top view of a test cell: (1) main U-frame, (2) collar, (3) clamping plate, (4) stress relief strip, (5) rubber gasket, (6) glass plate.

accommodated the thermocouple wires and power leads which were brought out at a right angle to the cylinder axis.

A second heat exchanger in connection with a different test cell was designed for circulating a working fluid from a constant temperature bath through the cylinder. Tap holes, 0.5 cm in diameter, were drilled axially into a 2.5 cm O.D. brass cylinder every 45° with their axes located on a 1.5 cm diameter circle. The two holes in the center provided the connection for the inlet and outlet tubes. The holes were selectively connected by grooves and closed by disks on each end of the cylinder. One disk was provided with three holes for connecting the inlet and outlet tubes and for bringing out the wires of the four thermocouples which were located at $\theta = 0°$, 90°, 180° and 270°, and installed as described before. A hole was drilled through the inner glass plate of the test cell for bringing out the fluid supply tubes and the thermocouple wires. After installation of the cylinder the holes were sealed with silicone-rubber cement to prevent the leakage of the liquid test material from the test cell.

Phase change material

Paraffins have been suggested as phase change materials for thermal energy storage systems which take advantage of the latent heat-of-fusion [11]. In this investigation *n*-heptadecane and *n*-octadecane were employed as the materials. *N*-heptadecane and *n*-octadecane, both with a purity of 99%, were purchased from Humphrey Chemical Company, North Haven, CT. Phase transition of *n*-paraffins has been studied in detail [13–15] and their transport, physical and optical properties are reasonably well documented. The data used in this study are tabulated elsewhere [10]. It should be noted that significant discrepancies may exist between literature sources reporting thermophysical property data for a particular paraffin. Differences may be due to purity, measurement techniques, data interpretation and measurement errors. *N*-heptadecane and *n*-octadecane were chosen as test materials because the liquid is transparent, thus allowing for optical and photographic observation of the melt zone. Their physical and transport properties are well established and thus facilitate the proper nondimensionalization, necessary in generalizing the results. In addition, their fusion temperatures were conducive for reducing heat losses from the test cell to the ambient laboratory environment.

Test procedure

Prior to each experiment the phase change material was heated to well above its fusion temperature until no rising gas bubbles could be visually observed (for the purpose of degasification). It was then cooled to about 5°C above the fusion temperature and syphoned into the test cell. The ambient air temperature was so controlled as to insure that only a small temperature difference existed between the air and the fusion temperature of the test material. Great care was taken to establish a uniform temperature of the material with very little subcooling, $(T_s - T_f)$. For example, before melting was initiated in the constant surface temperature experiment, ethylene glycol was circulated through the heat exchanger at a temperature of about 5°C below the fusion temperature of the material while it was still liquid to assure a firm solid layer around the heat source and to reduce the possibility of cavities above the heat exchanger. After all of the material was solidified, the temperature of the circulating fluid was raised to close to the fusion temperature of the material for the purpose of eliminating subcooling as a parameter on the melt shape and heat transfer. When the thermocouples located throughout the test cell indicated a temperature within 0.2°C of the imposed cylinder surface temperature, the preheating process was terminated. The initial condition, a uniform temperature of the solid close to the fusion temperature, was assumed to be established to begin the experiment.

For experiments in which the cylinder was heated electrically, the power supply for the cartridge heater was connected to a variable transformer and a wattmeter to control and maintain constant electrical power input to the heater. In determining the surface heat flux, the power input to the cylinder was corrected for the heat losses from the ends to the cell windows. This was accomplished by modeling the cylinder (brass tube with the electric cartridge heater) as an extended body, and using the measured surface temperature to estimate the end losses.

In experiments in which the heat exchanger was heated/cooled by circulating a fluid the inlet and outlet tubes of the heat exchanger were connected to a constant temperature bath. The temperature of the circulating fluid was controlled by a mercury contact thermoregulator.

The thermocouples were connected to an automatic integrating digital microvoltmeter and a high speed digital printer, which scanned the selected channels automatically, and printed the emf output at preselected time intervals. Photographs were taken of the screen with a 6 × 6 cm still camera (Mamiya C300 Professional) having a 250 mm f6.3 telelens. The camera recorded the solid–liquid interface position and displayed both time (LED digits) and length scales (cross hair and bullseye) on the negative.

RESULTS AND DISCUSSION

Cylinder surface temperature

Due to the design and the material of the heat sources for either boundary condition, the cylinder surface temperature was practically uniform in axial and polar directions. In the case of constant surface heat flux boundary condition, the wall temperature variation over the entire length of the cylinder was less than 0.4°C, while the variation with angular position never exceeded 0.2°C even for the largest surface heat flux. The maximum wall temperature typically occur-

red at the top of the cylinder ($\theta = 180°$). For the constant wall temperature boundary condition only 60 to 120 s were needed to reach a constant surface temperature [10]. Variations of $\pm 0.1°C$ were due to the temperature control of the constant temperature bath.

At $Ste_H = 0.996$ and $Ste_H = 0.755$, during constant surface heat flux experiments with *n*-octadecane, distinct "overshoots" in the wall temperature were noted at $Fo = 1.0$ and $Fo = 1.5$ [3]. The initial increase of the cylinder surface temperature, shortly after the power had been switched on, occurred during the period of time when natural convection effects were of secondary importance and conduction within the liquid layer surrounding the cylinder was the dominant mode of heat transfer; a regime which Grigull and Hauf [16] labeled as "pseudo-conductive". The occurrence of the peak surface temperature is considered to be associated with the change from the pseudo-conduction through transition to a fully developed natural convection regime. The gradual decrease of the surface temperature was caused by an intensification of natural convection circulation which continued until the flow became fully developed and the cylinder surface temperature reached a constant value. Similar types of temperature overshoots have been observed in transient natural convection heat transfer from a vertical plate [17], a horizontal wire [18] and in horizontal cylindrical annuli [19]. They also are expected for transient heating of a cylinder immersed in a liquid [20].

Solid–liquid interface motion

During each experiment photographs of the advancing solid–liquid interface were taken to study the shape and motion of the interface and to determine the melt volume during phase change heat transfer. Prints were made and liquid volume of the molten material was measured either with a planimeter or an automatic area meter.

Heat losses from the test cell were very small, which resulted in a uniform melting front in the axial direction. A set of solid–liquid interface positions for the constant surface heat flux boundary condition (q_w = const.) and with *n*-octadecane as phase change material is shown in Fig. 2. The melt shape is symmetric about the axis of the cylinder in the early stages of the process, $\tau_H = Ste_H \cdot Fo < 1.2$. The concentric liquid region around the cylinder indicates that heat transfer from the cylinder is primarily by conduction. After some time natural convection develops and intensifies, influencing the melt shape in general and the melt region above the cylinder in particular. Grigull and Hauf [16] found that in air ($Pr = 0.71$) even for Grashof numbers($Gr = g\beta(T_1 - T_2)(R_2 - R_1)^3/\nu^2$) as low as 470, in the so-called "pseudo-conductive" regime, a clearly identifiable convection pattern is evident.

A "pear-shape" like liquid region around the cylinder develops at $\tau_H > 1.2$ and elongates as heat addition

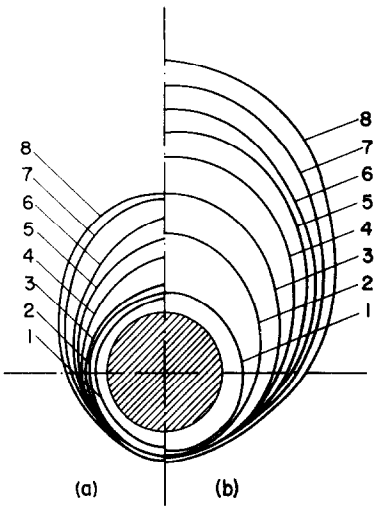

FIG. 2. Experimentally determined liquid region contours for *n*-octadecane [(1) $Fo = 0.96$, (2) $Fo = 1.92$, (3) $Fo = 2.28$, (4) $Fo = 3.84$, (5) $Fo = 4.8$, (6) $Fo = 5.76$, (7) $Fo = 6.72$, (8) $Fo = 7.68$]: (a) $Ste_H = 0.461$ and (b) $Ste_H = 0.996$.

to the material continues. At higher imposed wall heat fluxes and longer times, the flow pattern in the melt is sufficiently intense to affect the lower half of the melt region too. A thermal plume above the cylinder was observed [3] which oscillated and appeared to be three-dimensional in nature. An undisturbed, vertically oriented thermal plume in the liquid produces a circulation pattern during the melting process which is symmetric about a vertical plane through the cylinder axis. The plume conveys hot liquid to the upper part of the melt region and continues to support the upward movement of the interface. The circulation pattern was observed visually by following the motion of very small (less than 0.1 mm size) paraffin particles, most likely of higher molecular weight which were present in the melt. Oscillation of the plume above the cylinder was frequently observed but no definite periodicity could be established. Subcooling of the solid material was a distinct parameter which influenced the shape and size of the melt region. The parameter

$$S = \frac{c_s(T_f - T_i)}{\Delta h_f} \tag{1}$$

can be used as a measure of the importance of initial subcooling on the shape of the melt zone. This parameter never exceeded a value of 0.03 in the experiments and indicates that very little energy was required to bring *n*-octadecane to the fusion temperature as compared with the latent heat-of-fusion.

Effects of subcooling of the solid on the melt region around a heated horizontal cylinder were also reported by Abdel-Wahed *et al.* [4]. The melt region for the subcooled solid was substantially smaller than that without subcooling, because part of the energy input at the solid–liquid interface was absorbed as sensible heat by the solid. Also, the shape of the melt region was

observed to be narrower than that for no subcooling. Present findings support the results of their study.

Imposing a constant wall temperature on a cylinder embedded in *n*-heptadecane by circulating a working fluid through the heat exchanger at a temperature higher than the fusion temperature of the surrounding solid material resulted in liquid region contours [10] similar to those shown in Fig. 2. After an initial period, during which heat transfer in the melt is dominated by conduction, the circular solid–liquid interface changed to a "pear-shape" like form which indicated presence of natural convection in the liquid. An unsymmetrical shape of the melt region observed [10] was most likely due to a change in direction of the thermal plume. The origin of the plume shifted arbitrarily from $\theta = 180°$ to $\theta = 190°$ and impinged at the upper part of the solid–liquid boundary at about $\theta = 200°$. This caused a change in the natural convection circulation pattern and subsequently nonsymmetrical melting above the cylinder. The initial subcooling parameter S for this experiment was 0.0025. The results for the solid–liquid interface position support earlier statements that not only subcooling of the solid PCM but also the plume direction have a direct influence on the shape of the melt contour.

Inspection of Fig. 2 shows that melting takes place primarily above the cylinder, with very little occurring below. The strong upward thrust of the melting zone is caused by natural convection. As the Stefan number increases, the solid above the cylinder melts faster and affects the overall shape of the melt region. Sparrow *et al.* [2] and Abdel-Wahed *et al.* [4] have reported experiments on the role of natural convection during phase change. The experiments were performed with an eutectic mixture of sodium hydroxide and sodium nitrate. The heating cylinder was instrumented to provide information about the surface heat transfer coefficient, and a grid of 92 thermocouples was deployed throughout the phase change medium to detect the passage of the solid–liquid interface. Recently, Goldstein and Ramsey [9] have reported a set of data for solid–liquid naphthalene interface which was recorded photographically. Although the melt shapes are qualitatively similar, a direct comparison of the melt shapes is not possible because of different materials and thermal conditions used.

Heat transfer at the solid–liquid interface

To understand better the heat transfer processes in the melt a small Mach–Zehnder interferometer was used to visualize the temperature distributions and to infer the natural convection circulation in the liquid. The interferometer was of typical rectangular design and had 7.3 cm diameter optics. The test cell and the heat exchanger used are described elsewhere [21]. The sensitivity of the index of refraction of *n*-heptadecane to temperature made it very difficult to use the interferometer for quantitative measurements with reasonable surface to fusion temperature differences. A few degrees Celsius temperature difference resulted in too many fringes for accurate interpretation of the interferograms particularly when the melt layer was thin and/or natural convection in the melt was intense. For this reason the interferograms recorded are used here only for qualitative purposes.

Photographs of the interference fringes clearly show that at early times the fringes are concentric about the axis of the cylindrical heat exchanger. The fringe pattern indicates that conduction is the only mode of heat transfer, as was concluded by Beckman [22]. A selected photograph (Fig. 3) shows a melt region and a fringe pattern* which has already departed from a symmetric, annular one; particularly above the upper stagnation point between $\theta = 150°$ and $\theta = 210°$. Grigull and Hauf [16] have shown, using smoke tests, that even for Rayleigh numbers as low as 315 there is already natural convection present in the annulus. The interferogram supports their findings. In spite of the rather even spacings between the fringes, by this time the melt shape has departed from a circularly symmetric one. The small plume originating from the top of the cylinder has contributed to unsymmetrical melt front motion. This type of plume behavior was frequently observed during the experiments.

Figure 4 shows a fully developed natural convection circulation during phase change. The interference fringe pattern depends on shape and size of the melt region, and the cylinder surface temperature. The more intense the natural convection circulation in the melt the more pronounced is the recirculation which supports the melting above the heat source. The fringe density and, therefore, the temperature gradient at the upper stagnation point ($\theta = 180°$) is larger at the solid–liquid interface than on the cylinder surface. This clearly indicates a higher heat transfer rate at the interface than on the cylinder surface.

Based on a series of experiments with both constant heat flux and constant temperature boundary conditions at the cylinder surface, heat transfer coefficients at the solid–liquid interface were determined during melting. This was accomplished by analyzing interface motion during the phase change process. An instantaneous energy balance at the interface can be expressed as

$$\rho \Delta h_f \frac{dr}{dt} = h(T_w - T_f) + k_s \frac{\partial T_s}{\partial r}. \qquad (2)$$

The heat transfer coefficient at the melt boundary h can be deduced from the knowledge of the interface velocity (dr/dt) and the knowledge of the cylinder surface temperature T_w if heat conduction into the solid is small and can be neglected. This would occur when the temperature of the solid is close to its fusion

*The fluid inlet and outlet lines located at the lower stagnation point ($\theta = 0°$) prevented formation of the interference fringes on the lower part of the heat exchanger.

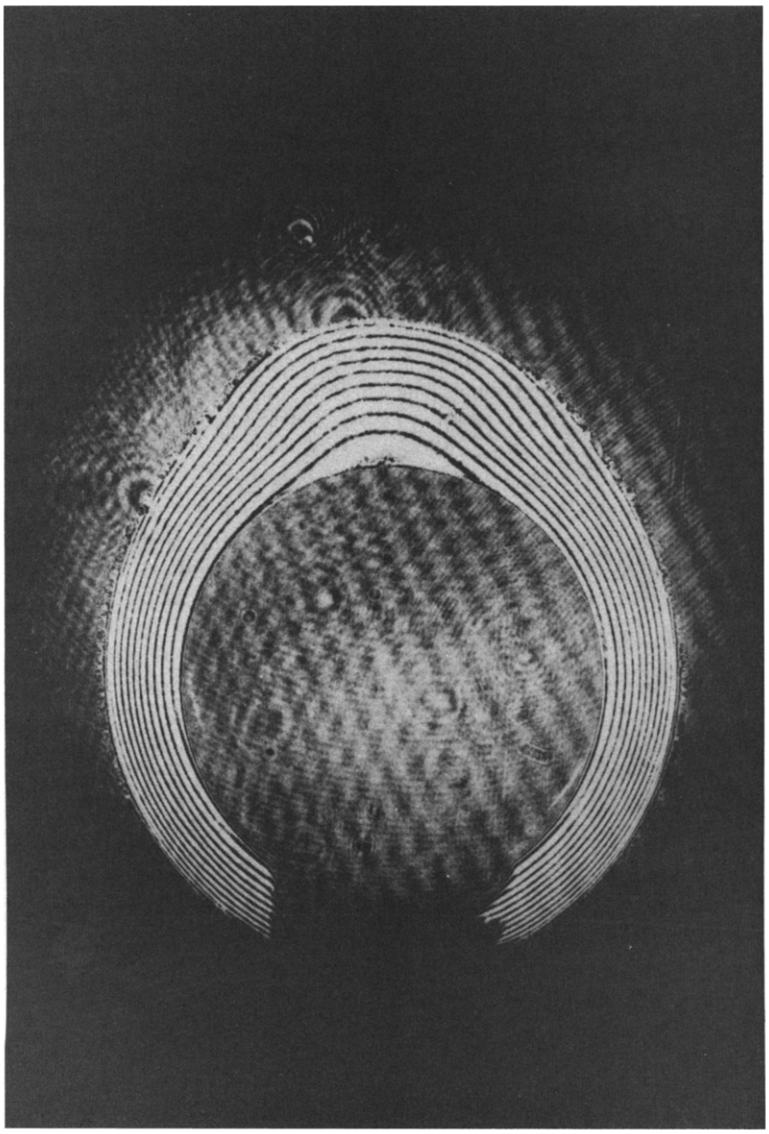

FIG. 3. Photograph of the interference fringe pattern in the liquid during melting of n-heptadecane surrounding a heated horizontal cylinder ($D_0 = 1.59$ cm), $T_w = 28.3\,^{\circ}$C.

temperature, i.e. negligible subcooling.

In each experiment the interface position was photographed as the melting progressed and the data was analyzed to determine dr/dt as a function of angular position θ and a time (Fig. 5). Since the remaining parameters in equation (2) are known or measured quantities, the local heat transfer coefficient was determined from the equation

$$h(\theta, t) = \frac{\rho \Delta h_f}{(T_w - T_f)} \left(\frac{dr}{dt}\right)_{\theta, t}. \quad (3)$$

For early times, when the melt layer was thin, it was difficult to determine dr/dt with sufficient accuracy, and therefore results were not obtained. The local heat transfer coefficients, determined from equation (3), showed little variation with time, possibly because by this time quasi-steady melting conditions were reached [2, 3, 5]. The heat transfer coefficients presented in Fig. 6 are effectively average values over the Fourier number range from about 0.5 to 8.0.

The dependence of the local heat transfer coefficient with the angular position and the boundary condition at the cylinder surface can be approximated by the empirical equation

$$h(\theta) = \frac{a}{Ste_l} + b \exp[-c(\pi - \theta)^2 (Ste_l)^{-1/2}] \quad (4)$$

where $a = 0.3\ \mathrm{W\,m^{-2}\,^{\circ}C^{-1}}$ and $c = 0.258$ are empirical constants and the constant b depends on the boundary condition at the cylinder surface, i.e. $b =$

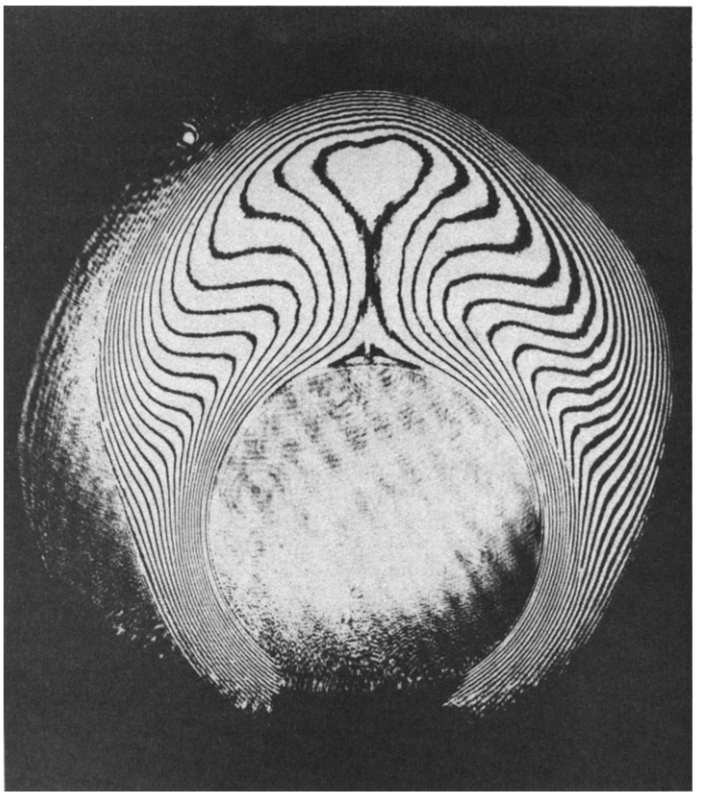

FIG. 4. Photograph of the interference fringe pattern in the liquid during melting of *n*-heptadecane surrounding a heated horizontal cylinder ($D_0 = 1.59$ cm), $T_w = 28.8\,^{\circ}C$.

$75\,W\,m^{-2}\,^{\circ}C^{-1}$ for $q_w = \text{const.}$ and $b = 80\,W\,m^{-2}\,^{\circ}C^{-1}$ for $T_w = \text{const.}$ The Stefan number Ste_l in equation (4) is independent of the boundary condition at the cylinder surface. The local heat transfer coefficients at the solid–liquid interface determined for the constant heat flux and for the constant surface temperature (see Fig. 6) boundary conditions show relatively little dependence on Ste_l and are almost independent of angular position θ in the range of $-60° < \theta < 60°$ for $q_w = \text{const.}$ and $-25° < \theta < 25°$ for $T_w = \text{const.}$ The quasi-steady local heat transfer coefficients given in Fig. 6 are consistent in trends with the results for the local heat flux through the liquid–solid naphthalene interface at different angular positions [9].

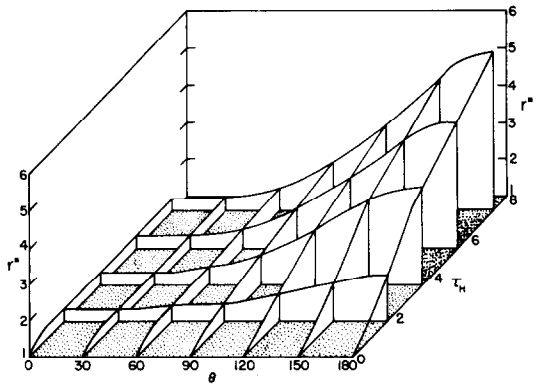

FIG. 5. Solid–liquid interface position as a function of angular position and time for *n*-octadecane, $Ste_H = 0.996$.

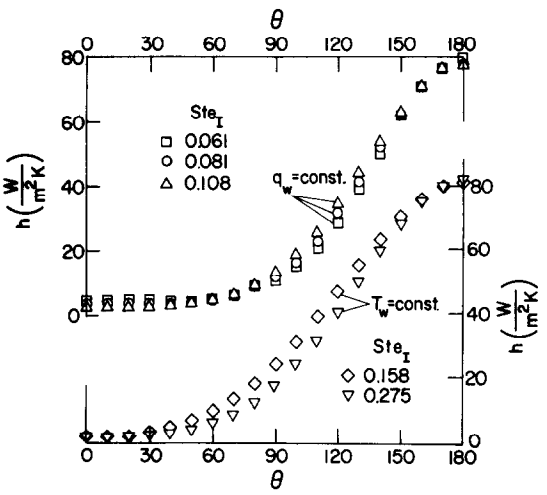

FIG. 6. Local heat transfer coefficient at the solid–liquid interface for constant surface heat flux (*n*-octadecane) and constant surface temperature (*n*-heptadecane) boundary conditions.

Correlation of natural convection heat transfer at the solid–liquid interface

Natural convection heat transfer from a horizontal cylinder and in horizontal cylindrical annuli have been studied and correlations have been proposed. Almost all of the correlations use the gap width δ as characteristic length in the Grashof and Nusselt numbers [23]. Itoh *et al.* [24] have proposed $\sqrt{(r_1 r_2)}\ln(r_2/r_1)$ as a characteristic length for the Grashof number, where the subscripts 1 and 2 refer to inner and outer radii of the annulus, respectively.

Analysis of the data obtained showed that the experimental results could be best correlated by basing the Nusselt and Grashof numbers on the characteristic radius R_c defined as

$$R_c = (r_m R_0)^{1/2} \ln(r_m/R_0) = R_0 B = R_0 (r_m^*)^{1/2} \ln r_m^*. \quad (5)$$

In this equation r_m is the mean interface radius based on perimeter $P\ (=2\pi r_m)$ (see Fig. 7) of the solid–liquid interface which defines the outer boundary of the liquid region. The parameter B is a correction factor for the "pear-shaped" melt region.

By choosing an abscissa which takes the Stefan number at the solid–liquid interface into account, the experimentally determined local Nusselt numbers at the interface for the prescribed boundary conditions at the cylinder surface are correlated by straight lines as shown in Fig. 8. The symbols indicate experimental data while the solid lines represent empirical equations of the form

$$Nu_{R_c} = C(Ra/Ste_l)^{1/3}, \quad (6)$$

where the constant C depends on the boundary condition. Comparison of the correlating equations with experimental results for mean Nusselt numbers at the solid–liquid interface is given in Fig. 9. For both the constant surface heat flux and constant surface temperature boundary conditions the experimental results can be approximated by the empirical equation

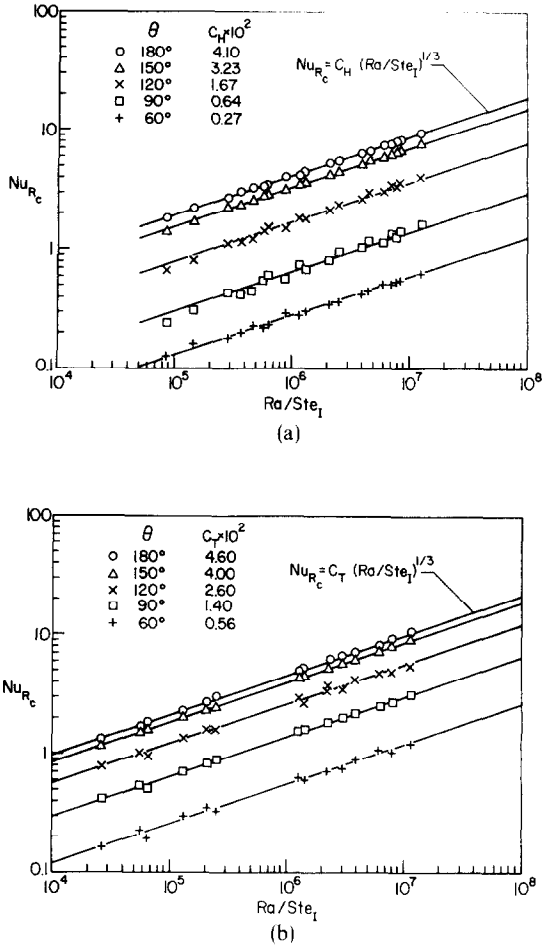

FIG. 8. Local Nusselt number at the solid–liquid interface: (a) constant surface heat flux (*n*-octadecane) and (b) constant surface temperature (*n*-heptadecane) boundary conditions.

$$\overline{Nu}_{R_c} = A(Ra/Ste_l)^{1/3} \quad (7)$$

where $A = 0.0178$ for $T_w = \text{const.}$ and $A = 0.0135$ for $q_w = \text{const.}$ boundary conditions.

Prediction of solid–liquid interface motion

In the analysis of systems or in fundamental studies of heat transfer with phase change it is desirable to

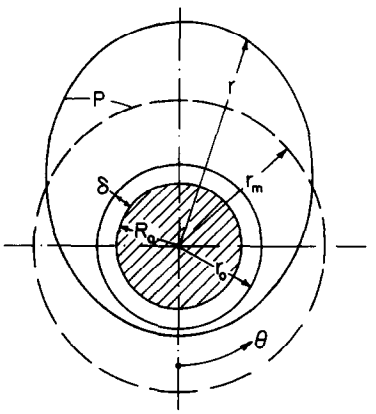

FIG. 7. Physical model and coordinate system of the melt region.

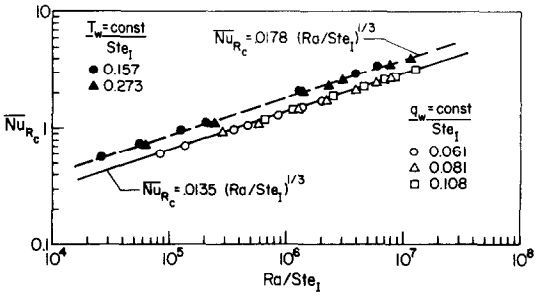

FIG. 9. Correlation of average Nusselt number at the solid–liquid interface.

predict the solid–liquid interface motion during melting of a material around a horizontal cylinder. Models which take into account natural convection heat transfer in the melt could not be found in the literature. The complexity of the equations, the nonlinearity introduced by the motion of the interface (which is not known *a priori*), and the departure of the melt region from a circular shape due to natural convection precludes closed form analytical solutions. Finite difference solutions appear possible but would be quite complicated. White *et al.* [1] used a perturbation method to approximate the problem for small Rayleigh numbers. Although a "pear-shape" like melted region around the cylinder was predicted after natural convection in the melt became dominant, the model did not yield realistic predictions when the melt front departed significantly from the circular shape.

To simplify the analysis in calculating the solid–liquid interface position, the following model is postulated. It is assumed that the subcooling of the solid is negligible and that during early phases of melting heat transfer is by conduction. During this phase of the melting process the melt region is symmetrical about the axis of the cylinder, and the position of the interface can be determined from analyses which consider conduction to be the only mode of heat transfer in the liquid [25–27]. The maximum gap width $\delta = r_0 - R_0$ (of the concentric melt region) is reached at time t_0 when natural convection begins to develop. For $t > t_0$ natural convection in the melt is sufficiently developed and the position of the interface is predicted from the equation

$$\rho \Delta h_f \frac{dr}{dt} = h(T_w - T_f), \quad t > t_0, \tag{8}$$

with the initial condition

$$r = r_0 \quad \text{at} \quad t = t_0. \tag{9}$$

Introduction of dimensionless variables and integration yields the result

$$r^* = r_0^* + \tfrac{1}{2} Nu(\tau_I - \tau_0) \tag{10}$$

where Nu is the local Nusselt number at the solid–liquid interface based on the cylinder diameter and the dimensionless time, $\tau_0 = Ste_I Fo_0$, corresponds to r_0^*. Assuming that the melt shape is symmetrical about a vertical plane through the cylinder axis yields the mean radius of the solid–liquid interface,

$$r_m^* = r_0^* + \tfrac{1}{2} \overline{Nu}(\tau_I - \tau_0), \tag{9}$$

where the average Nusselt number at the solid–liquid interface is given by

$$\overline{Nu} = \frac{D_0}{k}\left(\frac{a}{Ste_I} + 0.555\, b \sqrt[4]{(Ste_I)}\right) \tag{11}$$

if equation (4) is used for the local heat transfer coefficient.

It was determined from experimental data that the dimensionless time at which the interface was first observed to depart from a circular shape, $\tau_0 = Ste_I Fo_0$, depended on Ste_I and on the particular cylinder surface boundary condition. The value of this dimensionless time was $\tau_0 = 0.132$ for $q_w = $ const. and $\tau_0 = 0.0255$ for $T_w = $ const.

The gap width δ at $Fo = Fo_0$ was determined by employing the criteria that for the "pseudo-conductive" regime $Ra_\delta \leq 1700$ [16]. This was justified on the basis that for $0 < Fo \leq Fo_0$ the melt region was concentric about the heat source.

Figures 10 and 11 give comparisons between calculated and measured solid–liquid interface positions for $q_w = $ const. and $T_w = $ const., respectively. Results are shown only for an angular position $0° \leq \theta \leq 180°$, because it was assumed that the liquid region around the cylinder was symmetric about a vertical plane through the axis of the cylinder. As expected, for either cylinder surface boundary condition, the calculated and experimentally measured interface positions show good agreement. The greatest discrepancy between the two results occurred around the upper stagnation point ($\theta = 180°$). In general, at late times the interface position in the vicinity of $\theta = 180°$ is more difficult to calculate accurately because of arbitrary swaying of the thermal plume which may produce an unsymmetrical melt shape.

SUMMARY AND CONCLUSIONS

Melting from a horizontal embedded in *n*-paraffins produces an unsymmetrical melt zone around the heat source. This is due to the development of natural convection flow in the liquid. The local heat transfer

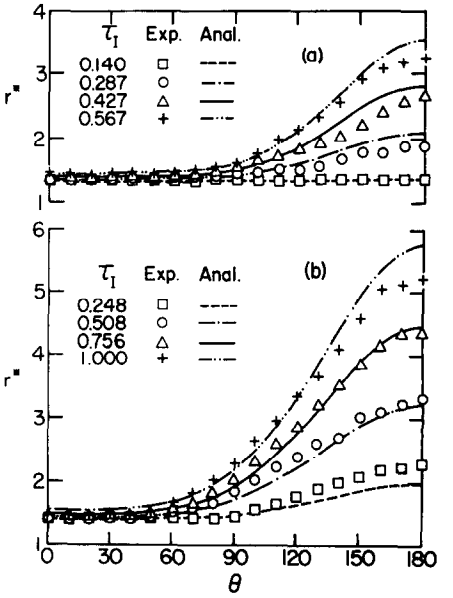

FIG. 10. Comparison between calculated and measured solid–liquid interface positions for melting of *n*-octadecane, $q_w = $ const.: (a) $Ste_H = 0.461$, $Ste_I = 0.061$ and (b) $Ste_H = 0.996$, $Ste_I = 0.108$.

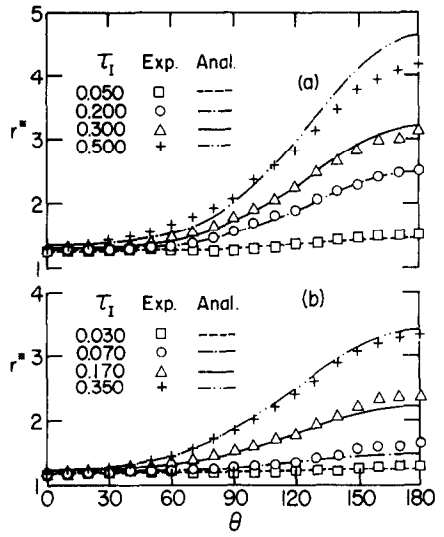

FIG. 11. Comparison between calculated and measured solid–liquid interface positions for melting of *n*-heptadecane, T_w = const.: (a) $Ste_T = Ste_I = 0.158$ and (b) $Ste_T = Ste_I = 0.275$.

coefficients at the solid–liquid interface were determined from the photographically recorded interface positions. For quasi-steady melting the local Nusselt numbers were correlated by an empirical equation of the form, $Nu = C(\theta)(Ra/Ste_I)^{1/3}$, and the average Nusselt numbers were correlated by the equation $\overline{Nu}_{R_c} = A(Ra/Ste_I)^{1/3}$. In these equations $C(\theta)$ and A are coefficients which depend on the boundary conditions imposed at the heat source surface.

The experimental results show that natural convection effects during melting are of first order importance and should be considered in any analysis of systems involving phase change. The knowledge of the heat transfer coefficient at the solid–liquid interface allows prediction of the interface motion.

The results reported have been obtained with a low thermal conductivity material. The empirical correlations obtained should be applied with caution to systems having different imposed thermal conditions and/or thermophysical properties. There is still a need for experimental data covering a much wider range of imposed thermal conditions and with materials having thermophysical properties much different than those studied. This information would be helpful in developing analyses and in their verification.

Acknowledgements – This work was supported by the National Science Foundation Heat Transfer Program under Grant No. ENG-7811686. The authors are indebted to Professor W. Leidenfrost for many helpful discussions.

REFERENCES

1. R. D. White, A. G. Bathelt, W. Leidenfrost and R. Viskanta, Study of heat transfer and melting from a cylinder imbedded in a phase change material, ASME Paper No. 77-HT-42 (1977).
2. E. M. Sparrow, R. R. Schmidt and J. W. Ramsey, Experiments on the role of natural convection in the melting of solids, *J. Heat Transfer* **100,** 11–16 (1978).
3. A. G. Bathelt, R. Viskanta and W. Leidenfrost, An experimental investigation of natural convection in the melted region around a heated horizontal cylinder, *J. Fluid Mech.* **90**(2), 227–239 (1979).
4. R. M. Abdel-Wahed, J. W. Ramsey and E. M. Sparrow, Photographic study of melting about an embedded horizontal heating cylinder, *Int. J. Heat Mass Transfer* **22,** 171–173 (1979).
5. A. G. Bathelt, R. Viskanta and W. Leidenfrost, Latent heat-of-fusion energy storage: Experiments on heat transfer from cylinders during melting, *J. Heat Transfer* **101,** 453–458 (1979).
6. J. W. Ramsey, E. M. Sparrow and L. M. C. Varejao, Melting about a horizontal row of heated cylinders, *J. Heat Transfer* **101,** 732–733 (1979).
7. J. W. Ramsey and E. M. Sparrow, Melting and natural convection due to a vertical embedded heater, *J. Heat Transfer* **100,** 368–370 (1978).
8. N. W. Hale, Jr. and R. Viskanta, Photographic observation of the solid–liquid interface motion during melting of a solid heated from an isothermal vertical wall, *Lett. Heat Mass Transfer* **5,** 329–337 (1978).
9. R. J. Goldstein and J. W. Ramsey, Heat transfer to a melting solid with application to thermal energy storage systems, in *Heat Transfer Studies: Festschrift for E. R. G. Eckert*, pp. 199–206. Hemisphere, New York (1979).
10. A. G. Bathelt, Experimental study of heat transfer during solid–liquid phase change around a horizontal heat source/sink, Ph.D. Thesis, Purdue University, School of Mechanical Engineering, West Lafayette, Indiana (1979).
11. H. G. Lorsch, K. W. Kauffman and J. C. Denton, Thermal energy storage for heating and off-peak air conditioning, *Energy Conversion* **15,** 1–8 (1975).
12. F. Kreith, *Principles of Heat Transfer*, 3rd ed. Intext Educational Publishers, New York (1976).
13. S. Takagi and K. Suzuki, The phase transition in *n*-paraffin, *Acta Crystallogr.* **7,** 697 (1954).
14. L. J. Thomas and J. W. Westwater, Microscopic study of solid–liquid interfaces during melting and freezing, *Chem. Engng Prog. Symp. Ser.* **59**(41), 155–164 (1963).
15. W. R. Turner, Normal alkanes, *Ind. Engng Chem., Prod. Res. Dev.* **10**(3), 238–260 (1971).
16. U. Grigull and W. Hauf, Natural convection in horizontal cylindrical annuli, in *Proceedings of the Third International Heat Transfer Conference*, Vol. 2, pp. 182–195, A. I. Ch. E., New York (1966).
17. R. J. Goldstein and E. R. G. Eckert, The steady and transient free convection boundary layer on a uniformly heated vertical plate, *Int. J. Heat Mass Transfer* **1,** 208–218 (1960).
18. J. R. Parsons and J. C. Mulligan, Transient free convection from a suddenly heated horizontal wire, *J. Heat Transfer* **100,** 423–428 (1978).
19. T. H. Kuehn and R. J. Goldstein, An experimental study of natural convection heat transfer in concentric and eccentric horizontal cylindrical annuli, *J. Heat Transfer* **100,** 635–640 (1978).
20. R. M. Fand and K. K. Keswani, Mass rate of flow in the natural convection plume above a heated horizontal cylinder immersed in a liquid, *J. Heat Transfer* **95,** 192–198 (1973).
21. A. G. Bathelt, P. D. Van Buren and R. Viskanta, Heat transfer during solidification around a cooled horizontal cylinder, *A. I. Ch. E. Symp. Ser., No. 189,* **75,** 103–111 (1979).
22. W. Beckmann, Die Wärmeüberstragung in zylindrischen gasschichten bei natürlicher konvection, *Forsch. Geb. IngWes.* **2,** 165–178 (1931).
23. T. H. Kuehn and R. J. Goldstein, Correlating equations

for natural convection heat transfer between horizontal circular cylinders, *Int. J. Heat Mass Transfer* **19**, 1127–1134 (1976).
24. M. Itoh, T. Fujita, N. Nishiwaki and M. Hirata, A new method of correlating heat transfer coefficients for natural convection in horizontal cylindrical annuli, *Int. J. Heat Mass Transfer* **13**, 1364–1368 (1970).
25. A. Horsthemke and E. Marschall, Speicherung von thermischer Energie in Salz- und Metallschmelzen, *Brennst.-Wärme- Kraft* **28**, 18–22 (1976).
26. N. Shamsundar and E. M. Sparrow, Analysis of multidimensional conduction phase change via the enthalpy model, *J. Heat Transfer* **97**, 333–340 (1976).
27. D. G. Wilson, A. D. Solomon and P. T. Boggs, *Moving Boundary Problems*. Academic Press, New York (1978).

TRANSFERT THERMIQUE A L'INTERFACE SOLIDE-LIQUIDE PENDANT LA FUSION A PARTIR D'UN CYLINDRE HORIZONTAL

Résumé—On étudie expérimentalement le transfert thermique pendant la fusion à partir d'une source de chaleur horizontale et cylindrique avec un flux surfacique uniforme (chauffage électrique) et une température de surface uniforme (chauffage par circulation d'un fluide à travers un échangeur de chaleur à plusieurs passes), noyée dans des n-paraffines (n-Heptadécane et n-Octadécane). La forme instantanée du volume fondu est enregistrée photographiquement et des coefficients locaux de transfert thermique à l'interface solide–liquide sont déterminés à partir de ces mesures. Pour la fusion quasi-stationnaire, les résultats sur le transfert de chaleur local et moyen sont présentés sous une forme adimensionnelle. En utilisant la formule ainsi déterminée, la position de l'interface solide–liquide est calculée et elle est trouvée en bon accord avec les données expérimentales.

WÄRMEÜBERGANG AN DER PHASENGRENZE FEST/FLÜSSIG BEIM SCHMELZEN AN EINEM WAAGERECHTEN ZYLINDER

Zusammenfassung—Der Wärmeübergang beim Schmelzen an einer waagerechten zylindrischen Wärmequelle mit konstanter Oberflächenwärmestromdichte (elektrisch beheizt) und konstanter Oberflächentemperatur (beheizt durch strömende Flüssigkeit in einem mehrgängigen Wärmetauscher) wurde experimentell mit *n*-Paraffinen (*n*-Heptadekan und *n*-Oktadekan), in welche die Wärmequelle eingebette war, untersucht. Die momentane Form des geschmolzenen Volumens wurde fotografisch festgehalten und daraus die örtlichen Wärmeübergangskoeffizienten an der Phasengrenze bestimmt. Für quasistationäres Schmelzen werden die örtlichen und mittleren Wärmeübergangskoeffizienten in dimensionsloser Form dargestellt. Mit der auf diese Weise bestimmten Beziehung wurde die Position der Phasengrenze berechnet. Der Vergleich zeigte gute Übereinstimmung mit den experimentell ermittelten Werten.

ТЕПЛОПЕРЕНОС НА ГРАНИЦЕ РАЗДЕЛА ТВЕРДОЕ ТЕЛО-ЖИДКОСТЬ ПРИ ПЛАВЛЕНИИ НА ГОРИЗОНТАЛЬНОМ ЦИЛИНДРЕ

Аннотация — Проведено экспериментальное исследование переноса тепла при плавлении на горизонтальном цилиндрическом источнике тепла при однородной плотности теплового потока (нагрев электрическим током) и однородной температуре поверхности (нагрев жидкостью, циркулирующей в многоходовом теплообменнике). Производилось фотографирование объёмов расплава и определялись локальные коэффициенты теплообмена на границе раздела твердое тело жидкость. Для квазистационарного плавления результаты по локальному и среднему теплообмену представлены в безразмерном виде. С помощью полученных таким образом соотношений рассчитывалось положение границы раздела твердое тело–жидкость. Результаты расчетов подтверждаются соответствующими экспериментальными данными.